

SgrA* spin and mass estimates through the detection of an extremely large mass-ratio inspiral

Verónica Vázquez-Aceves¹, Yiren Lin², Alejandro Torres-Orjuela³*

¹*Institute of Applied Mathematics, Academy of Mathematics and Systems Science, Chinese Academy of Sciences, 100190 Beijing, China.*

²*Astronomy Department, School of Physics, Peking University, Beijing 100871, China*

³*MOE Key Laboratory of TianQin Mission, TianQin Research Center for Gravitational Physics & School of Physics and Astronomy, Frontiers Science Center for TianQin, Gravitational Wave Research Center of CNSA, Sun Yat-Sen University (Zhuhai Campus), Zhuhai 519082, China*

Accepted XXX. Received YYY; in original form ZZZ

ABSTRACT

Estimating the spin of SgrA* is one of the current challenges we face in understanding the center of our Galaxy. In the present work, we show that detecting the gravitational waves (GWs) emitted by a brown dwarf inspiraling around SgrA* will allow us to measure the mass and the spin of SgrA* with unprecedented accuracy. Such systems are known as extremely large mass-ratio inspirals (XMRI) and are expected to be abundant and loud sources in our galactic center. We consider XMRI with a fixed orbital inclination and two scenarios for SgrA*'s spin (s): A highly spinning scenario where $s=0.9$ and a low spinning scenario where $s=0.1$. For both cases, we obtain the number of circular and eccentric XMRI expected to be detected by space-borne GW detectors like LISA and TianQin. We later perform a Fisher matrix analysis to show that by detecting a single XMRI the mass of SgrA* can be determined with an accuracy ranging from 0.06 to 3 solar masses while the spin can be measured with an accuracy between 1.5×10^{-7} and 4×10^{-4} .

Key words: black hole physics — gravitational waves — supermassive black holes – methods: analytical

1 INTRODUCTION

SgrA*, the super-massive black hole (SMBH) at our galactic center, was recently observed by the Event Horizon Telescope (Akiyama et al. 2022a,b,c,d,e,f) obtaining an estimated mass of $4 \times 10^6 M_{\odot}$, which is in good agreement with previous estimates (Ghez et al. 2008; Gillessen et al. 2009); in contrast, measuring its spin remains a major challenge. In this work we show that detecting a single extremely large mass ratio inspiral (XMRI), i.e., a brown dwarf (BD) inspiraling towards SgrA* due to energy loss by gravitational waves (GWs), is enough to determine the spin and mass of SgrA* with very good accuracy.

When an XMRI forms in our galactic center, its GW emission can be detected by space-borne detectors such as the Laser Interferometer Space Antenna (LISA) (Amaro-Seoane et al. 2017; Amaro-Seoane 2020) and TianQin (Luo et al. 2016; Mei et al. 2021). Furthermore, its large mass-ratio $q = m_{\text{BD}}/M_{\text{SgrA}^*} \approx 10^{-8}$, allows the BD to spend a large amount of time inspiraling around the SMBH, and the slow evolution of the orbit simplifies the analysis of its gravitational radiation. Understanding its formation channels and evolution is a key part of the description that will lead to accurate templates to identify and extract the information encoded within its gravitational radiation.

In a dense stellar system, such as our galactic center, two-body relaxation processes slowly change the orbits of the orbiting objects by diffusion in energy and angular momentum (J). However, as dif-

fusion in J is more efficient than diffusion in energy, the eccentricity (e) of the orbits changes faster than the semimajor axis (a). As a consequence, the pericentre (R_p) of the orbit is perturbed, allowing objects to reach very close distances to the central black hole. An inspiraling system is formed when a compact object is diffused into an orbit with a small R_p such that after just one pericentre passage the orbit evolves only due to the energy lost by gravitational radiation.

Recent estimates show that at the time the LISA and TianQin missions will be in space, there could be about 15 eccentric and five circular XMRI in our galactic center emitting GWs in a detectable range Amaro-Seoane (2019). In section 2, we compute the number of circular ($e \lesssim 0.2$) and eccentric ($e \gtrsim 0.9$) sources that will be present in the LISA/TianQin band in the cases in which the spin (s) of SgrA* takes a value of 0.1 and 0.9. The XMRI considered in the present work are composed of BDs inspiraling in prograde orbits with a fixed orbital inclination of $i = 0.1$ rad. In Section 3, we perform a Fisher matrix analysis of the systems described in Section 2 and show, for each spin case, how accurately we can measure the mass and spin of SgrA* by detecting an individual XMRI either in the eccentric or in the circular regime.

2 NUMBER OF XMRI IN THE CENTER OF OUR GALAXY

To estimate the number of XMRI in the center of our galaxy for different values of the spin and inclinations, we first estimate the event rates $\dot{\Gamma}_{\text{XMRI}}$ as in Amaro-Seoane (2019) by integrating those sources

* E-mail: atorreso@mail.sysu.edu.cn (ATO)

of which the orbits evolve only due to GW emission in phase space. Such systems have a semimajor axis $a \lesssim a_{\text{crit}}$, where a_{crit} marks the critical distance at which the system reaches an internal energy that shields the binary against relaxation processes; for XMRI a_{crit} is of the order of $\sim 10^{-2}$ pc to 10^{-3} pc depending on the spin of the SMBH. The event rates for these sources are given by

$$\dot{\Gamma}_{\text{XMRI}} = \frac{3}{5T_0} \frac{N_{\text{IR}}}{R_{\text{h}}^\lambda} f_{\text{sub}} \left\{ \left[a_{\text{crit}}^\lambda \left(\ln \left(\frac{a_{\text{crit}}}{2R_{\text{LSO}}} \right) - \frac{1}{\lambda} \right) \right] \right\}, \quad (1)$$

where $\lambda = 5/4$, $N_{\text{IR}} = M_{\text{SgrA}^*}/\bar{m}$ is the number of objects within the influence radius of SgrA*, $R_{\text{h}} \approx 3$ pc, $T_0 \approx 29 \times 10^9$ yr is a normalization timescale, R_{LSO} is the position of the last stable orbit (LSO), $\bar{m} = 0.27 M_\odot$ is the average stellar mass, and $f_{\text{sub}} = 0.21$ is the fraction number of BDs. The last two quantities, \bar{m} and f_{sub} , are obtained from a Kroupa broken power law (Kroupa 2001). For a Kerr black hole, the position of the LSO is $R_{\text{LSO}} = 4 R_{\text{S}} \mathcal{W}(i, s)$, where the effect of the spin and inclination with respect to the spin axis is included through the function $\mathcal{W}(i, s)$ (Teukolsky & Shapiro 1983; Amaro-Seoane et al. 2013) and $R_{\text{S}} = 2GM/c^2$ is the Schwarzschild radius, G is the gravitational constant, and c is the speed of light in vacuum.

The position of the LSO is shifted depending on the spin magnitude; an object orbiting around a Kerr black hole in a prograde orbit finds that the LSO is shifted towards the Schwarzschild radius so it can reach closer distances to the SMBH. Consequently, an XMRI formed around a SMBH with high spin can reach smaller pericentre distances, and higher eccentricities, compared to an XMRI formed around a slowly spinning SMBH. Furthermore, there is a limit to the eccentricity that an XMRI can have. This limit is given by

$$e_{\text{max}} = 1 - \frac{R_{\text{LSO}}}{a}, \quad (2)$$

if a compact object approaches a SMBH in an orbit with $e > e_{\text{max}}$, it crosses the LSO at pericentre and suffers a direct plunge.

Equation (1) assumes that BDs are part of the light stellar component in the central part of the galaxy and that they distribute around SgrA* following the same stellar density distribution as main sequence (MS) stars, i.e., a power-law cusp $\rho(r) \approx r^{-7/4}$ (Bahcall & Wolf 1976). For this reason Equation (1) is only valid for XMRI or objects that follow the distribution of MS stars (see Amaro-Seoane (2019) for more details).

Once an XMRI is formed, it will orbit SgrA* for around 10^8 years. The merger timescale (T_{GW}) is given by

$$T_{\text{GW}} = \frac{10}{64} \frac{a^4 c^5}{G^3 m M^2} f(e), \quad (3)$$

where

$$f(e) = (1 - e^2)^{7/2} \left[1 + \frac{73}{24} e^2 + \frac{37}{96} e^4 \right]^{-1}, \quad (4)$$

with $m = m_{\text{BD}}$, and $M = M_{\text{SgrA}^*}$. Equation (3) applies to systems with $M \gg m$ and where the pericentre remains approximately constant during the inspiral process, which is suitable for cases where $e \approx 1$ as we are considering here (Peters 1964).

The total number of XMRI N_{tot} orbiting around SgrA* can be estimated by multiplying the event rate $\dot{\Gamma}_{\text{XMRI}}$ obtained for a given value of a_{crit} by the merger timescale

$$N_{\text{tot}} = \dot{\Gamma}_{\text{XMRI}}(a_{\text{crit}}) \times T_{\text{GW}}. \quad (5)$$

This equation includes all the sources with a semimajor axis between the plunge radius $a_{\text{plunge}} \approx R_{\text{S}}$ and a_{crit} , but does not take into

SgrA* spin	e	$\dot{\Gamma}_{\text{XMRI}}$ [yr^{-1}]	N_{I}	N_{II}
0.1	0.999	1.306×10^{-7}	2	30
0.9	0.9999	1.181×10^{-6}	2	49

Table 1. Event rates ($\dot{\Gamma}_{\text{XMRI}}$), and number of circular sources (N_{I}) and eccentric sources (N_{II}) in band for XMRI with a fixed orbital inclination of $i = 0.1$ rad and an eccentricity $e \approx e_{\text{max}}$ for two different spin values.

account if the GWs emitted by the system are within the detection band of space-borne detectors.

To obtain the number of sources within the detection band we follow the procedure presented in Amaro-Seoane (2019) and define a_{band} as the semimajor axis at which the XMRI is already in the detection band and a_{break} as the semimajor axis that separates the eccentric and circular regime: if $a \lesssim a_{\text{break}}$ the XMRI is already circularized, on the contrary, if $a \gtrsim a_{\text{break}}$ the XMRI is considered highly eccentric ($e > 0.9$). The number of circular sources is given by N_{I} and the number of eccentric sources by N_{II} ,

$$N_{\text{I}} = \frac{N_{\text{tot}}}{1 + [c_2 (1 + c_1)]^{-1}}, \quad (6)$$

$$N_{\text{II}} = N_{\text{tot}} - N_{\text{I}}, \quad (7)$$

where

$$c_1 = \frac{a_{\text{crit}}^{1/2} - a_{\text{band}}^{1/2}}{a_{\text{band}}^{1/2} - a_{\text{break}}^{1/2}}, \quad (8)$$

$$c_2 = \frac{1 - (a_{\text{plunge}}/a_{\text{break}})^4}{8 \left((a_{\text{crit}}/a_{\text{break}})^{1/2} - 1 \right)}. \quad (9)$$

To perform our analysis on the spin and mass of SgrA*, we consider XMRI formed by a BD of $0.05 M_\odot$ (Amaro-Seoane 2019) in a prograde orbit with an orbital inclination of $i = 0.1$ rad, which maximizes the value of the event rates, and we focus on two representative spin values: $s = 0.1$ and $s = 0.9$.

XMRI can form with different eccentricities as long as its eccentricity fulfils $e \lesssim e_{\text{max}}$ (cf. Equation 2), and its semimajor axis is smaller than the critical semimajor axis. The estimates given by Equations (6) and (7) depend on the initial eccentricity of the source. We choose initial eccentricity values close to the maximum eccentricity with which an XMRI can form in a prograde orbit around a Kerr SgrA* (Vázquez-Aceves et al. 2022), and compute the number of sources using the relation $R_{\text{p}} = a \times (1 - e)$ while setting $e_{\text{break}} = 0.2$, $R_{\text{break}} = 4 R_{\text{S}}$, $e_{\text{band}} = 0.9$, and $R_{\text{band}} = 5 R_{\text{S}}$. With these orbital parameters, sources in the circular regime have a Signal to Noise Ratio (SNR) of $\gtrsim 1,200$, while for the eccentric regime the SNR is around 50. We obtain $N_{\text{I}} \approx 2$ in the circular regime for both spin values, $N_{\text{II}} \approx 49$ in the eccentric regime for $s = 0.9$, and $N_{\text{II}} \approx 30$ for $s = 0.1$. See Table 1 for a summary of our results.

In the next section, we study how accurately we can measure the mass and spin of SgrA* by detecting a single XMRI, which represents a lower limit according to our estimates for N_{I} and N_{II} . A detailed study on the number of sources in the LISA/TianQin band with different inclinations, and the accuracy we can achieve on the measurements of the mass and spin by detecting multiple XMRI, will be published by the current authors soon elsewhere.

3 MEASURING THE SPIN AND MASS OF SgrA*

As mentioned in the previous section the XMRI we study have a SNR well above the typical detection threshold for comparable

sources (Babak et al. 2017). Therefore, we estimate how accurately the spin and the mass of SgrA* can be measured by performing a Fisher matrix analysis (Coe 2009), which provides a linearized estimate for the measurement errors that asymptotes to the true errors in the high-SNR limit. Having the waveform of the XMRI $h(\theta)$, where θ are the intrinsic and extrinsic parameters of the source, the Fisher matrix can be defined as

$$\Gamma_{i,j} := \left\langle \frac{\partial h(\theta)}{\partial \theta_i}, \frac{\partial h(\theta)}{\partial \theta_j} \right\rangle. \quad (10)$$

Here $\langle \cdot, \cdot \rangle$ represents the noise-weighted inner product (Finn 1992; Klein et al. 2016). The inverse of the Fisher matrix $C := \Gamma^{-1}$ then approximates the sample covariance matrix of the Bayesian posterior distribution for the parameters given the observed signals.

A more detailed study of the measurability of the spin would involve analyses such as in Cutler & Vallisneri (2007) or full posterior sampling (Li 2013). However, we only intend to estimate the accuracy with which the spin of the SMBH in the center of our galaxy can be measured. Moreover, considering the very high SNR of the XMRI the Fisher matrix analysis provides very good estimates and thus we stick to the analysis introduced above.

We generate the waveform for the XMRI using a code based on Barack & Cutler (2004) and Fang & Huang (2020) expanding the rate of change of the orbital frequency and eccentricity to 2.5 post-Newtonian (PN) order while considering the effect of the spin of the SMBH through the pericentre precession and the Lense-Thirring precession to effectively 1.5 PN order. Restricting our analysis to lower PN orders reduces the computational costs and allows us to include a higher number of modes which is crucial due to the high eccentricity of the orbit and the sensitivity of space-based detectors (Amaro-Seoane et al. 2017; Luo et al. 2016).

Recent results from the Event Horizon Telescope (Akiyama et al. 2022a,b,c,d,e,f) indicate that the spin of SgrA* is pointing at a small angle ($\leq \pi/6$ rad) towards Earth. Therefore, we consider the case where the spin of SgrA* is aligned with the line-of-sight for the two cases introduced in Section 2: a low spin of 0.1 and a high spin of 0.9. For each spin value we consider two different eccentricity scenarios: i) an almost circular one with an eccentricity $e = 0.2$ and a pericentre distance $R_p = 4 R_S$, and ii) a very eccentric one with an eccentricity $e = 0.9$ and a pericentre distance $R_p = 5 R_S$. For the more circular case, we consider the first seven modes while for the more eccentric one we consider a total of 50 modes ($n = 49 - 98$) which are the modes that have the highest SNR in the detection band of LISA. We set SgrA* to have a mass of $4 \times 10^6 M_\odot$ and to be located at a distance of 8 kpc from Earth, and for both cases we set the mass of the BD to be $0.05 M_\odot$, consider its orbit to have an inclination of 0.1 rad, and an observation time of two years.

Figure 1 shows the accuracy for the measurement of the mass and spin of SgrA* with an almost circular XMRI. We see that for a high spin of 0.9 the mass is measured with an accuracy of $0.06 M_\odot$ while the spin can be measured with an accuracy of 1.4×10^{-7} . For a low spin of 0.1, the mass and the spin can be measured with slightly better accuracy of around $0.05 M_\odot$ for the mass and around 1.25×10^{-7} for the spin. The accuracy for the measurement of the mass and the spin of SgrA* from an XMRI with higher eccentricity (corresponding to higher event ratios) is shown in Figure 2. In this case, the accuracy of the measurement goes down but the mass still can be measured with an accuracy of around $3 M_\odot$ while the spin can be measured with an accuracy of (still astonishing) 4×10^{-4} , almost independent from the magnitude of the spin. For all cases considered, we further see that there is a strong correlation between the mass and the spin thus

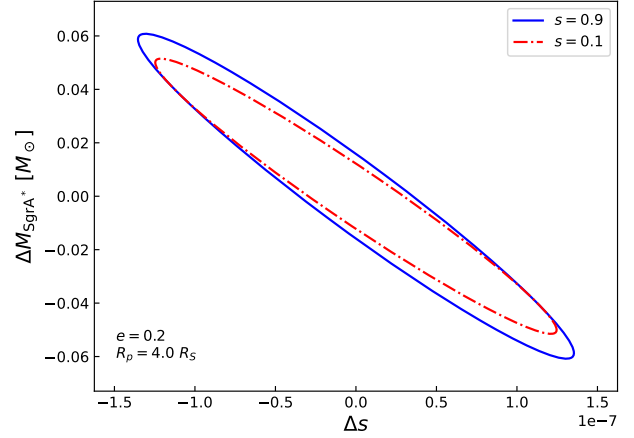


Figure 1. Accuracy for the measurement of the mass and the spin of SgrA* for an almost circular XMRI ($e = 0.2$, $R_p = 4 R_S$). The blue solid line corresponds to a spin of 0.9 while the red dash-dotted line corresponds to a spin of 0.1.

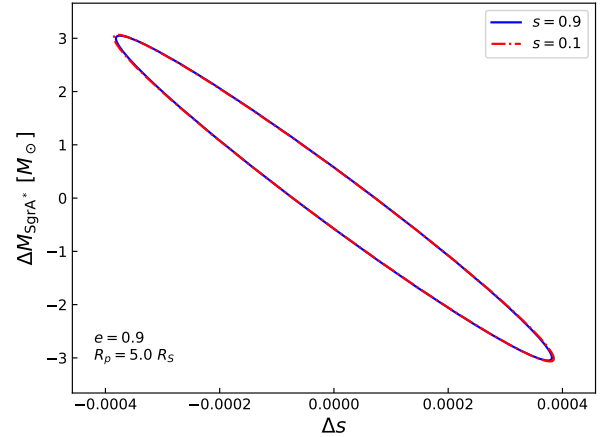


Figure 2. Accuracy for the measurement of the mass and the spin of SgrA* for a highly eccentric XMRI ($e = 0.9$, $R_p = 5 R_S$). The blue solid line corresponds to a spin of 0.9 while the red dash-dotted line corresponds to a spin of 0.1.

highlighting again the importance of the measurement of the spin of SgrA*.

4 CONCLUSIONS

XMRI have quite recently been proposed as a new kind of source for space-borne detectors such as LISA or TianQin (Amaro-Seoane 2019). Due to the small mass of the secondary compact object (the BD) these sources will only be detectable in the close universe. However, we expect them to be abundant and most likely, the loudest sources in our galaxy reaching easily a SNR of over 1000. Considering a fixed orbital inclination of $i = 0.1$ rad, we estimate the number of XMRI that space-borne detectors will be able to detect when

launched, finding that for almost circular orbits around two XMRI will be in band independently of the spin of SgrA* and that for highly eccentric orbits tens of XMRI will be in band with higher numbers for higher spins.

Using a waveform model based on Barack & Cutler (2004) and considering multiple modes of the GW, we perform a Fisher matrix analysis to estimate how accurately the mass and the spin of SgrA* can be measured from the detection of one XMRI. We find that for highly eccentric orbits the mass will be measured with an accuracy of around $3 M_{\odot}$ and the spin with an accuracy of 4×10^{-4} almost independent of the magnitude of the spin. For almost circular orbits and a high spin of 0.9, the mass will be detected with an accuracy of $0.06 M_{\odot}$ and the spin with an accuracy of around 1.5×10^{-7} . We obtain a slightly better accuracy of $0.05 M_{\odot}$ for the mass and of 1.25×10^{-7} for the spin when $s = 0.1$.

Future space-borne missions will detect XMRI with different orbital inclinations. Additionally, the population of XMRI in the LISA/TianQin band is related to SgrA*'s spin magnitude. As there is currently no restriction on the magnitude of the spin of SgrA*, in a follow-up paper that will be published soon elsewhere, we extend this study to different orbital inclinations and spin values to provide an insight into the accuracy with which we can measure the mass and the spin of SgrA*. Furthermore, we highlight that in this work we focus on the mass and spin of SgrA* because they are the two most important parameters of a SMBH. However, the astonishing accuracy that can be achieved detecting only one XMRI and considering that multiple XMRI will be in band when LISA/TianQin are launched, shows that XMRI are very promising sources for detailed studies of SgrA* and the fundamental physics of SMBHs.

ACKNOWLEDGEMENTS

We thank Pau Amaro-Seoane for helping us with his expertise on the formation and properties of XMRI. We further thank Xian Chen for helpful discussions. VVA acknowledges support from CAS-TWAS President's Ph.D. Fellowship Program of the Chinese Academy of Sciences & The World Academy of Sciences. YL is supported by the National Science Foundation of China (Grant No. 11873022) and the National Key Research and Development Program of China (Grant No. 2021YFC2203002). ATO acknowledges support from the Guangdong Major Project of Basic and Applied Basic Research (Grant No. 2019B030302001).

DATA AVAILABILITY

The data underlying this article will be shared on reasonable request to the corresponding author.

REFERENCES

- Akiyama K., et al., 2022a, *ApJ*, **930**, L12
Akiyama K., et al., 2022b, *ApJ*, **930**, L13
Akiyama K., et al., 2022c, *ApJ*, **930**, L14
Akiyama K., et al., 2022d, *ApJ*, **930**, L15
Akiyama K., et al., 2022e, *ApJ*, **930**, L16
Akiyama K., et al., 2022f, *ApJ*, **930**, L17
Amaro-Seoane P., 2019, *Phys. Rev. D*, **99**, 123025
Amaro-Seoane P., 2020, The gravitational capture of compact objects by massive black holes ([arXiv:2011.03059](https://arxiv.org/abs/2011.03059))
Amaro-Seoane P., Sopuerta C. F., Freitag M. D., 2013, *MNRAS*, **429**, 3155
Amaro-Seoane P., et al., 2017, preprint, ([arXiv:1702.00786](https://arxiv.org/abs/1702.00786))
Babak S., et al., 2017, *Phys. Rev. D*, **95**, 103012
Bahcall J. N., Wolf R. A., 1976, *ApJ*, **209**, 214
Barack L., Cutler C., 2004, *Phys. Rev. D*, **69**, 082005
Coe D., 2009, arXiv e-prints, p. [arXiv:0906.4123](https://arxiv.org/abs/0906.4123)
Cutler C., Vallisneri M., 2007, *Phys. Rev. D*, **76**, 104018
Fang Y., Huang Q.-G., 2020, *Phys. Rev. D*, **102**, 104002
Finn L. S., 1992, *Phys. Rev. D*, **46**, 5236
Ghez A. M., et al., 2008, *ApJ*, **689**, 1044
Gillessen S., Eisenhauer F., Trippe S., Alexander T., Genzel R., Martins F., Ott T., 2009, *ApJ*, **692**, 1075
Klein A., et al., 2016, *Phys. Rev. D*, **93**, 024003
Kroupa P., 2001, *MNRAS*, **322**, 231
Li T. G. F., 2013, PhD thesis, Vrije Universiteit Amsterdam
Luo J., et al., 2016, *Classical and Quantum Gravity*, **33**, 035010
Mei J., et al., 2021, *Progress of Theoretical and Experimental Physics*, **2021**, 05A107
Peters P. C., 1964, *Phys. Rev.*, **136**, B1224
Teukolsky S., Shapiro S., 1983, *Black holes, white dwarfs, and neutron stars : the physics of compact objects*. Wiley
Vázquez-Aceves V., Zwick L., Bortolas E., Capelo P. R., Amaro Seoane P., Mayer L., Chen X., 2022, *MNRAS*, **510**, 2379

This paper has been typeset from a $\text{\TeX}/\text{\LaTeX}$ file prepared by the author.